Published in final edited form as:
Magn Reson Imaging. 2013 October ; 31(8): 1349–1359. doi:10.1016/j.mri.2013.05.003.

A Comparison and Evaluation of Reduced-FOV Methods for Multi-Slice 7 Tesla Human Imaging

Christopher J. Wargo[1,2], **Jay Moore**[1,2], and **John C. Gore**[1,2]

[1]Institute of Imaging Science, Vanderbilt University, 1161 21st Ave. South, MCN AA-1105, Nashville, TN 37232-2310. USA

[2]Department of Radiology and Radiological Sciences, Vanderbilt University, 116 21st Ave. South, MCN CCC-1106, Nashville, TN 37232-2675, USA

Abstract

Eight different reduced field-of-view (FOV) MRI techniques suitable for high field human imaging were implemented, optimized, and evaluated at 7 Tesla. These included selective Inner-Volume Imaging (IVI) based methods, and Outer-Volume Suppression (OVS) techniques, some of which were previously unexplored at ultra-high fields. Design considerations included use of selective composite excitation and adiabatic refocusing radio-frequency (RF) pulses to address B1 inhomogeneities, twice-refocused spin echo techniques, frequency-modulated pulses to sharply define suppressed regions, and pulse sequence designs to improve SNR in multi-slice scans. The different methods were quantitatively compared in phantoms and *in vivo* human brain images to provide measurements of relative signal to noise ratio (SNR), power deposition (specific absorption rate, SAR), suppression of signal, artifact strength and prevalence, and general image quality. Multi-slice signal losses in out-of-slice locations were simulated for IVI methods, and then measured experimentally across a range of slice numbers. Corrections for B1 nonuniformities demonstrated an improved SNR and a reduction in artifact power in the reduced-FOV, but produced an elevated SAR. Multi-slice sequences with reordering of pulses in traditional and twice-refocused IVI techniques demonstrated an improved SNR compared to conventional methods. The combined results provide a basis for use of reduced-FOV techniques for human imaging localized to a small FOV at 7 T.

1. INTRODUCTION

Reduced-FOV imaging acquires data from small regions of interest within an object to diminish the size of image matrices. Typically, using a FOV smaller than the object induces an aliasing or fold-over artifact that adversely affects image quality because the Nyquist sampling criterion are not satisfied. This artifact is prevented using reduced-FOV methods by isolating excitation to within a localized region only. To accomplish this, two general approaches are commonly applied: selective excitation methods that excite only the region of interest using multiple pulses for localization such as Inner-Volume Imaging (IVI) [1], and suppression-based methods that apply bands to saturate signal external to the target

Corresponding Author: Christopher J. Wargo, chris.wargo@vanderbilt.edu, Fax: (615) 322-0734, Phone: (615) 343-0466.

FOV prior to excitation, such as Outer-Volume Suppression (OVS), and B1 Insensitive Train to Obliterate Signal (BISTRO) [2–4].

Reduced-FOV methods are challenged by the decreased SNR due to using a smaller FOV (and, usually, voxel) size, the need for adequate suppression of signal from outside the FOV to prevent aliasing, in some cases, the introduction of additional RF pulses that increase power deposition (specific absorption rate, SAR), and may necessitate additional scan preparation. IVI techniques also suffer additional signal losses in multi-slice scans that rely on the intersection of pulses along multiple dimensions. Each phase encoding pulse acts on spins in all neighboring slices, with insufficient time for full magnetization recovery after each pulse to ensure maximum signal when sampled. A number of methods attempt to partially or fully correct for this loss, but introduce additional constraints on the applied scan parameters [5–9].

To date, the majority of reduced-FOV methods have been implemented at field strengths ranging from 0.35 T to 3T, for diverse applications that include localization of cardiac structures and diffusion tensor imaging (DTI) in the spinal cord [2, 10–12]. Specific applications at 7T have been less fully demonstrated [4, 13–17] but the additional signal strength measurable at high fields provides new opportunities for high resolution imaging of small FOVs in reasonable times. High-resolution imaging necessitates that a large array of data be acquired dependent on the object size, increasing scan times. Longer acquisition times constrain the temporal resolution for functional studies, and can result in greater degradation from physiological and motion based artifacts, as well as signal blurring and distortion induced by susceptibility effects, especially for single-shot echo planar imaging (EPI) scans. Rapid imaging methods such as parallel imaging [18], compressed sensing [19], and partial Fourier acquisitions [20, 21] have countered these effects by diminishing data sizes, echo train lengths, and the occurrence of motion artifacts. Reduced-FOV approaches are capable of similar data reductions and provide comparable improvements in scan time or spatial resolution.

Implementing reduced-FOV at 7 T for high resolution faces a number of additional challenges caused by field dependent effects, such as increased B1 inhomogeneity, higher power deposition (SAR), and changes in relaxation parameters. A number of solutions to alleviate inhomogeneity problems have been developed using alternate RF designs, such as composite and adiabatic pulses [22–24], parallel transmission [25, 26], and spatial-spectral excitation techniques such as “spokes” [27]. To become useful methods at 7T in practice, reduced-FOV techniques require optimization within the constraints of ultra-high field. Here, we demonstrate the implementation and optimization of IVI and OVS based reduced-FOV for T2 weighted human imaging at 7T using EPI. To address B1 inhomogeneity constraints, composite and adiabatic pulses were explored. Additional solutions to signal losses for IVI multi-slice scans were also investigated. The performances of all optimized techniques were compared to evaluate relative SNR, suppression of unwanted signal, SAR, residual artifacts, and sensitivity to B1 variation.

2. METHODS

2.1. Selective Excitation and Suppression Based Reduced-FOV Techniques

a. Method 1: Inner-Volume Imaging (IVI)—Inner-Volume Imaging (IVI) was implemented as described by Feinberg [1] (Figure 1A) using a pair of RF pulses selective in orthogonal directions to achieve reduced-FOV localization. Magnetization is refocused only in a volume where the two applied pulses intersect. The implemented IVI differs from that described previously [1] by using an excitation pulse selective along the x-dimension, followed by a slice selective refocusing pulse with balanced crushers. Pulse shape and

duration for each were optimized to minimize pass-band and side-band ripple artifacts, with sharp edge transitions in between. The 90° excitation consisted of a five-lobe SINC pulse with a 15 μT amplitude and 3.92 ms duration, with the 180° refocusing accomplished with a two-lobe SINC with 15 μT amplitude and 5.40 ms duration, for a minimum TE of 16 ms.

b. Method 2: Inner-Volume Imaging Using Composite Excitation (CE-IVI)—To achieve a reduction in B1 inhomogeneity caused by spatial variations in flip angles at high field strength, IVI was modified to use a composite RF pulse for slice selective excitation [23, 24, 28] and a refocusing pulse in the orthogonal direction with an adiabatic shape (Figure 1B). The composite consisted of eight Gaussian pulses each with 1.06 ms durations with 22 mT/m trapezoid gradients to achieve a 4 mm slice thickness. A minimization algorithm was used to iteratively adjust the individual pulse amplitudes and phases, with the flip angle at each iteration compared against a target to calculate error. Local minimization was obtained when the difference in angle error was below a defined threshold. The applied non-linear constrained minimization algorithm used a maximum B1 of 15 μT and pulse duration limits based on hardware constraints, with the range of ΔB_0 and B1 defined from values measured in human brain and phantoms at 7T. The total duration for the composite pulse was 12 ms, 12.8 ms for the adiabatic refocusing pulse set to a 180° using a 15 μT amplitude, resulting in a minimum TE value of 24 ms with the combined RF waveforms.

c. Method 3: Outer-Volume Suppression (OVS) Using a Frequency Modulated RF Pulse—Outer-Volume Suppression (OVS) [2, 4, 12, 17] was developed to apply two 10 cm suppression bands that targeted regions left and right of the reduced-FOV region (Figure 1C). The pulse pairs were repeated twice to enhance signal suppression with band placement achieved by setting the individual offset frequencies, Δf_o, for each pulse:

$$\Delta f_0 = \pm BW / \left(\left(w_{slab} - \frac{w_{rfov}}{2} \right) G_{PE} \gamma \right) \quad (1)$$

BW corresponds to the bandwidth of the suppression pulse, G_{PE} the active gradient strength to generate slab width w_{slab}, with the phase encoding dimension reduced to w_{rfov}. Signal was dephased between each pulse pair using 40 mT/m spoiling gradients. For each RF pulse, a numerically optimized chirp pulse [29] with a linear frequency modulation (FM) was used to achieve a quadratic phase profile [2, 4, 30, 31], with a 160° flip angle for the first pulse repetition, and 90° for the second, labeled α_1 and α_2 (Figure 1C). This resulted in peak amplitudes of 8.32 μT and 15 μT, respectively, with 8.63 ms durations, 3.9 kHz bandwidths, for a time-bandwidth product (TBW) of 38, and total OVS time of 76 ms. A single gradient was applied to generate both suppression bands and to serve as spoiling between each RF pulse. To reduce B1 inhomogeneity, the composite and adiabatic pulses described previously were used in the spin echo EPI sequence after OVS.

d. Method 4: B1 Insensitive Train to Obliterate Signal (BISTRO)—Similar localization using suppression bands for reduced-FOV was accomplished with the B1 Insensitive Train to Obliterate Signal (BISTRO) method described by Luo [3]. As shown (Figure 1D), BISTRO performs multiple repetitions of individual hyperbolic secant pulses that excite suppression regions left or right of the target reduced-FOV. The amplitudes of each pulse are scaled along the first half of a hyperbolic secant profile to diminish sensitivity to B1 inhomogeneity that would cause poor suppression:

$$B_n = B_N \operatorname{sech}(\beta(1 - n(t)/N) \quad (2)$$

N corresponds to the total number of pulses, n(t) the pulse number occurring at time t, B_N the maximum B1 amplitude, with β defining the profile shape. Eight pulses were applied left and right of the target reduced-FOV, for sixteen pulses total, with the left and right repetitions interleaved. Pulse durations were set to 5.6 ms and generate a 75 mm wide suppression band, using a maximum B1 amplitude of 15 μT, with a total BISTRO time of 103 ms. A single gradient that was selective in the phase encoding direction was applied to define the suppression bands, and additional short spoilers set to 40 mT/m were added between each secant pulse. The FM profile of every other pulse was reversed in direction to prevent unwanted echo formation, and a composite excitation and adiabatic refocusing was used for the spin echo EPI sequence following BISTRO to improve B1 uniformity.

2.2. Reduced-FOV Approaches to Prevent Multi-Slice Imaging Signal Loss

a. Method 5: ZOnally Oblique Method (ZOOM)—The Zonally Oblique Method (ZOOM) was implemented [9] (Figure 1E) to improve IVI signal performance when used with multi-slice scans. ZOOM reduces effects on the magnetization in neighboring slices by rotating the excitation by a specific angle. In the off-slice locations, this oblique orientation will only affect spins that are external to the desired reduced-FOV, preserving full magnetization in the reduced-FOV region when the neighboring slice is imaged as long as a specific slice gap is maintained. For this approach, the 90° excitation pulse was orthogonal to the slice direction with its gradients obliquely rotated instead of the 180° gradients as described by Symms [32].

The angle and width of the rotated plane in combination with the slice selective refocusing pulse were optimized for two configurations: to generate a 42 mm wide slab in a 210 × 210 mm^2 FOV, and to fully excite a 60 × 60 mm^2 reduced-FOV. Limitations of this technique include a required slice gap that is at least twice the slice thickness, and production of a transition band at the edge of the excited region where signal is lowered that necessitates additional oversampling to prevent fold-over into the reduced-FOV. Optimizing to a 5 mm slice gap and a 5 mm transition band required 67° and 74° angles for the two configurations, respectively, with the excitation band configured to be 16 mm wide in the phase encoding direction. All other aspects of the IVI were the same as described for the initial IVI approach without composite excitation.

b. Method 6: Multi-Slice IVI Using Double Refocusing (MS-IVI)—The approach of Jeong [5] using two refocusing pulses with IVI was implemented to reduce signal loss for multi-slice scans (Figure 1F). Here, a second 180° pulse is performed immediately after readout to restore the magnetization that was inverted by the first refocusing pulse. Taking into account loss in signal as a result of T1 recovery in the time between the two 180° pulses, it is predicted 70–80% of the signal will be maintained versus 20–30% without the additional pulse. Implementation of this method consisted of using the composite excitation and an adiabatic 180° pulse with balanced crushers for the first refocusing pulse. For the second, a short duration, two lobe SINC pulse that was asymmetrical was applied without crushers. The width of this pulse was set to affect a region twice that of the initial refocusing to reduce pass-band artifacts from the combination of the two. The pulse timing otherwise matched that for composite IVI.

c. Method 7: Twice-Refocused Acquisition to Constrain Excitation (TRACE)—A variant of MS-IVI was implemented (Figure 1G) using a combination of MS-IVI [5, 33], Continuously Oblique ZOOM (CO-ZOOM) [7], and Point Resolved Spectroscopy (PRESS) [34]. The CO-ZOOM approach applies a twice-refocused spin echo sequence with DTI and optimized gradients to reduce eddy current effects with reduced-FOV [35]. Using two refocusing pulses prior to readout with CO-ZOOM serves to realign the inverted spins in the

off-slice positions along the z-direction for optimal orientation to prevent signal loss. Realigning earlier in the scan compared to MS-IVI further reduces loss due to reduced T1 recovery between the first and second 180° while off-slice spins are inverted, producing higher signal levels.

The implemented approach used this concept to improve reduced-FOV imaging specifically for multi-slice scans. The timing was organized based on PRESS, with the separation between the initial excitation and refocusing pulses minimized based on RF and gradient limits. The spacing of the two refocusing pulses accounted for this initial delay and the duration between the final 180° and echo formation at readout. Orientation for each pulse was based on defining a reduced-FOV, twice refocusing off-slice positions, and minimizing pass-band artifacts where pulses overlapped. The initial excitation and refocusing pulses were both slice selective, with 90° pulse set to the target slice thickness, and the first 180° covering a volume that included all neighboring slices imaged. The final refocusing pulse was selective in the x-dimension, twice inverting off-slice positions. Composite and adiabatic pulses were used for excitation and refocusing, respectively, to improve B1 homogeneity, for a minimum TE of 45 ms. This method was uniquely specified as Twice Refocused Acquisition for Constrained Excitation (TRACE).

d. Method 8: IVI Using Two-Dimensional Spiral Rectangular Excitation (2DRF-IVI)—Simultaneous excitations constrained in orthogonal directions were accomplished by replacing the initial 90° excitation with a two-dimensional RF pulse (2DRF). Previous applications of 2DRF have aimed to confine excitation to prevent the impact on off-slice locations [5–8, 10, 36]. Here, the target excitation profile followed the formulation described by Pauly and Hardy [37, 38], using a 2D rectangular weighting function in the x-z plane, W(k), excited along a spiral trajectory (Figure 1H). Rectangle dimensions were defined by σ_z and σ_x, weighted by a Gaussian Hanning window, h(k), and scaled by α to achieve the target flip angle:

$$W(k)=h(k)\alpha\mathrm{sinc}(\sigma_x k_x)\mathrm{sinc}(\sigma_z k_z) \quad (3)$$

$$h(k)=e^{-\beta^2(k_z^2+k_x^2)} \quad (4)$$

The defined spiral trajectory consisted of 20 rotations with a maximal gradient strength of 36 mT/m with gradients terminating at zero to ensure the pulse is self-refocusing. The resulting B1 to achieve 2D rectangular excitation had a duration of 14.5 ms with a peak amplitude of 2.5 μT to establish a 90° flip angle in a 42 mm wide, 7 mm thick rectangle. To accomplish positioning of the rectangle in the slice dimension, the pulse was frequency modulated by a scaled version of the spiral waveform matching the shape of the slice direction gradient [39]. The 2DRF was followed by a slice selective 180° pulse between matched crusher gradients, resulting in a minimum echo time of 18.5 ms.

3. EXPERIMENTAL METHODS

3.1. Imaging Experiments for Reduced-FOV Method Comparisons

Comparisons between all eight methods were performed using a human Philips 7T Achieva system (Philips Healthcare, Cleveland, Ohio) with a 90 cm Magnex magnet, a Nova head array with 32 channels for reception (Nova Medical, Wilmington, MA), and a quadrature volume coil for transmission. Systems gradient strength, slew rate, and coil B1 peak amplitude were constrained to 40 mT/m, 200 mT/m/ms, and 15 μT, respectively.

Three image sets were collected to evaluate and compare the methods (Table 1) that included: 1.) use of each method to excite a 42 mm wide slab in a full-FOV scan, 2.) use of each method to reduce the FOV to 60 mm × 60 mm, and 3.) use of each multi-slice method to reduce the FOV to 60 mm × 60 mm FOV with the number of slices incrementally increased from 1 to 9. For experiment two, reduction in the readout direction was accomplished using bandpass filtering. For the multi-slice test, ZOOM, MS-IVI, TRACE, and IVI were each performed with the composite pulse modified to a SINC to reduce SAR, and MS-IVI repeated without the second refocusing pulse to serve as a baseline measure of SNR. Multi-slice acquisitions were further compared by simulating in Matlab (Mathworks, Natick, MA) the loss in off-slice magnetization for each method, using a TR of 2500 ms, 9 slices, a T1 of 50 ms, and T2 of 25 ms.

Experimental images were first obtained of a Functional Biomedical Information Research Network (FBIRN) phantom composed of agar gel with a 20 cm spherical diameter used in prior studies to assess stability of MRI systems [40] and to assess B1 inhomogeneity solutions [24], and then repeated using scans of the human brain in a healthy subject. Informed consent was obtained prior to human scans per an Institutional Review Board protocol approved by the Vanderbilt University Medical Center (Nashville, TN). For both the phantom and human scans, additional full FOV images without reduced-FOV were obtained, as well as 32 “images” of noise only with no active RF. All human scans were additionally configured to use fat suppression by applying Spectral Presaturation with Inversion Recovery (SPIR) set to a 500 Hz frequency offset.

3.3. Description of Reduced-FOV Method Analysis Metrics

a. Signal-to-Noise Ratio and Percent Suppression Measurement—To measure Signal-to-Noise Ratio (SNR) in all images, the image intensity at each pixel location, s(i,j), was divided by the standard deviation across the 32 “noise” acquisitions at the same location, σ(i,j). The calculated SNR was expressed as a percentage of the maximum SNR measured using the normal full-FOV scan, SNR_{max}:

$$SNR(i,j)=100\left(\frac{(s(i,j)/\sigma(i,j)}{SNR_{\max}}\right) \quad (5)$$

For the slab images, the percent suppression external to the slab, SP, was obtained by taking the image difference between the full-FOV and reduced-FOV slab images, (S_{full} and S_{slab}), expressed as a percentage of the full signal, where 100% is full suppression:

$$SP=100\left(\frac{S_{full}-S_{slab}}{S_{full}}\right) \quad (6)$$

b. Artifact Power Measurement—Artifact power (AP) maps were calculated from the absolute value of the squared difference between the reduced-FOV images, S_{rfov}, and the expected slab intensity, S_{base}. For the expected signal measured in the FBIRN, a mask was generated with equal intensity within the defined slab, for the expected human image, the full-FOV brain image was used. To account for SNR difference between scans, the mean AP value was subtracted from each map across all N pixels where it was measured. All reduced-FOV AP maps were expressed as a percentage of the maximum AP in the full-FOV data set:

$$AP_{rfov} = \left| \sqrt{\frac{(S_{rfov} - S_{base})^2}{(S_{base})^2}} \right| - \frac{1}{N} \sum_{j=1}^{N} \left| \sqrt{\frac{(S_{rfov}(j) - S_{base}(j))^2}{(S_{base}(j))^2}} \right| \quad (7)$$

c. SAR and Mean Statistics Analysis—For each acquisition, the scanner calculated SAR value was recorded and expressed as a percentage of the 3 W/kg limit for the head. The mean SNR and AP values were calculated for each method by selecting a region of interest (ROI) within the area selected by the reduced-FOV approach, excluding edges where differences in signal roll-off may be significant. For slab data, mean suppression was calculated for object regions external to the central 42 mm area excluding the image background. For the multi-slice data, the mean SNR was calculated for each method and number of slices combination, normalized as a percentage of the SNR with only 1 slice acquired.

4. RESULTS

4.1. Comparison of Reduced-FOV Methods for Slab Excitations

Slab excitations using each reduced-FOV method are presented in Figure 2 and 3 for phantom and human scans, respectively, image statistics are summarized in Figure 4, and profiles are displayed in Figure 5. Overall, each method successfully defined the target slab, with suppression levels above 94% in the FBIRN, lowest for OVS and BISTRO. In the human, suppression was generally diminished (91% to 95%) but uniform, dropping most significantly for OVS (83%), with poor suppression visible for OVS in a region of high signal dropout in both the phantom and human. Compared to the full-FOV scan in the phantom, reduced-FOV methods produced SNR that was 7% to 34% higher and artifact power that was 20% to 40% lower. For human imaging, SNR remained greater for all reduced-FOV methods except BISTRO. Artifact power was highest in the human using the spiral pulse at 60% above all other methods. Methods using B1 corrective pulses were 8% to 15% lower in AP than those without. Higher AP with the 2DRF may be attributed to visible distortion on each slab end, with a slight ripple artifact in the spiral slice profile (Figure 5). However, the rectangular profile excited along the slice dimension appeared sharply defined within the 7 mm thickness. Likewise, the matching profile for ZOOM visibly demonstrated the achieved transition band, which did not produce a substantially diffuse boundary for the ZOOM slab, though AP was elevated for ZOOM in the human. Overall, signal appeared to have greater uniformity for methods using the composite and adiabatic pulse, diminishing central dropout, with the remaining matching the quality of the full scan.

4.2. Comparison of Reduced-FOV Methods in a Small FOV

Small FOV excitations are presented in Figure 6 and 7, with statistics summarized in Figure 8. Qualitatively, the human images had consistent contrast with no visible artifacts that would indicate aliasing. In comparison, the FBIRN data had visible differences in signal intensity, with the full-FOV scan having significant dropout in the center of the FOV, lessened but visible for IVI without B1 correction, but absent in those using the composite and adiabatic combination. This was also reflected in the SNR maps. Additionally, there were no visible fold-over artifacts in the FBIRN images with the exception of OVS and BISTRO, which had slight ripple and edge effects, respectively. SNR was consistent between FBIRN and human scans, lowered to 43% to 68% of the full scan, highest with TRACE (a 53% drop in SNR was expected due to a reduction in the FOV size by a factor of 3.5 ($1/\sqrt{R}$)). Artifact power was consistently lower for all reduced-FOV methods compared to the full scans in the FBIRN, at 46% to 96%, and between 12% and 33% of the spiral IVI

for the human scans. As with the slab imaging, human artifact power was lowest for those scans using composite excitation and adiabatic refocusing by as much as 20%. Lastly, SAR was highest with OVS and BISTRO at 48% and 91%, with methods using composite and adiabatic pulses (CE-IVI, MS-IVI, and TRACE) between 15% and 30%, and all others below 9%.

4.3. Comparison of Reduced-FOV Methods for Multi-Slice Scans

The simulated and measured SNR for multi-slice scans using reduced-FOV are presented in Figure 9 in both the FBIRN and human. All three had agreement in the relative SNR between the methods tested. IVI using an initial 90° pulse that is slice selective as described by Feinberg [1] simulated and measured to have the highest drop-off in SNR as the number of slices increased to nine, to 60% and 22% in the FBIRN and human, respectively. Modifying the IVI to first use a pulse that is phase-encoding selective doubled SNR in the human, and increased phantom SNR by 18%. This improved by additional 5–15% using a second refocusing pulse after readout (MS-IVI), and a further 10–15% by moving the additional pulse prior to readout (TRACE). Lastly, SNR in the phantom with ZOOM maintained full SNR with increment in slice number, and a constant 10% drop in the human. The relative differences in SNR are reflected in the images at nine slices (Figure 10), with slice selective IVI significantly degraded by noise and an alternate contrast compared to the ZOOM, TRACE, and MS-IVI methods.

5. DISCUSSION

Application of reduced-FOV techniques for human brain imaging at 7T requires managing the impact of field inhomogeneity on RF performance to selectively localize or suppress signal. Significant reduction in suppression levels or compounding errors in pulse flip angle resulting from the combination of excitation and refocusing pulses selective along multiple dimensions can substantially degrade image quality within the reduced-FOV. Here, the combination of composite excitation and adiabatic refocusing produced a measured improvement in SNR, a lowering of artifact power, and an increase in signal uniformity within the reduced-FOV compared to a full-FOV without these techniques. Many of the techniques optimized with alternate pulse shapes also performed better than the full scan, suggesting the selected pulses were an improvement over those chosen as standard. The implementations described for the CE-IVI, MS-IVI, and TRACE inner-volume approaches differ from prior methods largely due to the combined application of these pulses, with adiabatic waveforms previously used primarily for spin echo, spectroscopy, and diffusion weighted imaging [22, 33, 41].

As demonstrated, a benefit of the selective composite pulse, beyond achieving improved B1 uniformity, is an insensitivity to change in the B1 profile across patients [23], eliminating the need to use B1 mapping methods commonly applied by multi-transmit approaches for RF shimming [42]. Adiabatic pulses are similarly relatively insensitive to B1 variation; however, they also introduce a quadratic phase distribution that results in signal loss when used for refocusing. The reduced-FOV designs developed here that apply a single pulse for adiabatic refocusing (MS-IVI, CE-IVI) addressed this constraint by using the adiabatic to select along the phase-encoding dimension only, which prevents any signal loss due to the phase effect. Likewise, using two adiabatic pulses that act orthogonally as described for TRACE achieves phase refocusing and negligible loss of signal [43]. In contrast, both OVS and BISTRO applied a single adiabatic for refocusing that was slice selective and showed the expected sensitivity to the quadratic phase. Despite this, both demonstrated improved SNR over the full scan with traditional pulses in the phantom, with only BISTRO lower in the human. This result suggests a compromise between improved refocusing performance and phase induced signal loss. Alternate adiabatic designs could be explored to improve

SNR [44], but can greatly elevate SAR beyond the high levels already observed using the composite and adiabatic pulses described. These pulses additionally constrain the minimum TE due to long durations, especially when repeated to achieve localization or to reduce multi-slice loss. Parallel transmit methods offer potential solutions to minimize such durations for pulses used for RF shimming [26], but was not available for the 7T system used here.

For suppression-based approaches, field inhomogeneity challenges the level of signal attenuation that is generated in regions that would otherwise alias into the reduced-FOV. Both techniques were optimized to maximize signal suppression in the suppression band regions within this constraint. The described OVS design, to our knowledge, represents a unique configuration in terms of the number of pulses, timings, and shapes to achieve reduced-FOV localization at 7T. The frequency modulated pulse applied here suggests a superior suppression to the von Morze OVS design that uses a quadratic phase pulse for diffusion-weighted imaging at 7T, with potentially a 6% to 10% higher suppression in a wider band using the FM pulse [4]. The FM waveform also provided sharp delineation of signal at the edges of the selected reduced-FOV.

Compared to BISTRO, which was configured to match closely to that described previously for 7T [3], OVS demonstrated a greater sensitivity to B1 variation. This was visible in a region of signal dropout caused by inhomogeneous B1, where lowered OVS suppression levels in both the phantom and human were observed. BISTRO maintained uniform suppression in that same region, benefiting from the use of multiple adiabatic pulses. Despite these differences in this region, both of which generated lower suppression than the IVI approaches, there was no visible aliasing artifact in the human scans in a small FOV across all methods, indicating suppression levels were sufficient. The primary constraint with OVS and BISTRO are an elevated SAR due to the high number of RF pulses, 40% to 90% above the other methods, with BISTRO twice that of OVS. The comparable performance in a small-FOV within the human brain suggests diminished benefit to using the higher SAR method BISTRO over OVS.

For multi-slice imaging, our analysis provides the first direct comparison between selective reduced-FOV methods, and distinct differences in performance were observed. Compared to prior approaches, a number of unique improvements resulted in diminished signal loss by adjusting pulse orderings and configurations [1, 5, 45]. Initiating IVI with a phase encoding excitation doubled the SNR in humans versus using an initial slice selective pulse as is commonly applied for IVI [1]. Inspecting the magnetization profile through simulation, this improvement is expected as a result of the off-slice position recovering from a 90° excitation at an earlier time instead of a full inversion using the traditional pulse order, enabling greater signal T1 recovery. The SNR loss with the reordered method was additionally measured to be only 4% and 12% below the Jeong technique (MS-IVI) which used a second refocusing pulse to further diminish SNR losses with IVI [12], observed here in phantom and human images, respectively.

Further reorganizing the twice-refocusing strategy to place the second 180 prior to readout with TRACE improved SNR beyond MS-IVI, to an 8% loss in the FBIRN, and 28% loss in human. Here, earlier twice refocusing provided a greater duration for T1 recovery before off-slice acquisition. Overall, TRACE results suggest that it is an improvement over prior methods due to the observed superior SNR for multi-slice scans. TRACE specifically differs from the multi-slice IMIV technique developed for diffusion weighted imaging in a reduced-FOV [33] that uses two adiabatic refocusing pulses, by adjusting the refocusing pulses to act on orthogonal directions, optimizing TRACE for T2 weighted anatomical imaging with a composite pulse, and minimizing the duration between excitation and the first refocusing

pulse to improve the minimum echo time. As described, TRACE also produced SNR in slab excitations and small FOV human scans in a single slice that was as much as 34% higher than the other methods, with artifacts comparable too or less than these techniques. Artifact power generally reflected the degree of signal variation caused primarily by B1 inhomogeneity, with high AP indicative of high variation. TRACE, however, produced four times the SAR level than IVI, and constrains imaging parameters compared to MS-IVI due to both refocusing pulses occurring prior to readout with ample spacing required for proper echo formation.

Overall, the analysis demonstrates the compromises necessary between reduced-FOV approaches. In the context of multi-slice imaging, a reordered IVI diminishes SNR compared to other methods but not as substantially as the traditional IVI; however, it enables greater flexibility in TR and TE values and the number of contiguous slices in a multi-slice protocol due to lower SAR without an extra refocusing pulse. Similar flexibility is achieved using the ZOOM approach, which produces no SNR loss with appropriate selection of pulse rotation parameters. We managed a transition band smaller than previously reported [32, 45] at 5 mm with minimal impact on the edge signal for the reduced-FOV. However, ZOOM necessitates a slice gap twice that of the slice profile width. Applying a 5 mm gap for our scans was slightly less than required, resulting in a constant 10% loss in SNR across all numbers of slices for human imaging.

The 2DRF pulse enables similar maintenance of SNR with multi-slice scans, with excitation well localized within the 7mm profile achieved. With this width, this method also necessitates a slice gap; 1.5 mm for the 4 mm slice thickness imaged here. Narrower profiles would require a broader gap to prevent impact to off-slice positions. Optimizing the 2DRF design to less than 7 mm is challenged by constraints on the gradient strength and pulse duration to prevent peripheral nerve stimulation and eddy currents, as well as the need for apodization to reduce ripple effects that broadens the 2D pulse profile. Both the ZOOM and 2DRF approaches also require optimization of a larger set of parameters to achieve different reduced-FOV sizes compared to standard IVI.

OVS and BISTRO are capable alternatives, producing no off-slice SNR loss for multi-slice scans, but limit the number of slices in a single multi-slice package due to high SAR. The MS-IVI and TRACE methods have lower power constraints than OVS and BISTRO, compromise SNR less than IVI, do not require a slice gap or transition band as with ZOOM and 2DRF, and are readily configured to any target FOV size. TRACE additionally produced superior SNR in the human than the other approaches, and diminished artifact power suggesting better B1 uniformity, but with a longer echo time. Each method is expected to have benefits for different applications based on the specific imaging constraints. The IVI methods with higher TE limits and pulses organized in a spin echo configuration are primarily suited for T2 or diffusion weighting, whereas OVS and BISTRO have greater flexibility with contrast and scan type, but are SAR limited. The implementation and analysis described here provide an approach for such uses at 7T.

6. CONCLUSIONS

To conclude, this study describes the first implementation of various reduced-FOV approaches for imaging at 7T. This analysis also provides the first comparison of relative performance of each implemented technique in the context of 7T anatomical imaging with unique solutions to B1 inhomogeneity problems and multi-slice signal loss, while providing insight into relative signal performance, suppression, and artifact power. The described implementations, comparison, and assessment serve as a basis for reduced-FOV use in a broad range of human imaging studies at 7 Tesla.

Acknowledgments

This work is supported by NIH grant number R01EB000461 and Training Grant number T32EB001628. The authors acknowledge Dr. Marcin Jankiewicz of the Vanderbilt University Institute of Imaging Science (VUIIS) for his assistance with implementation of 2D spiral excitation. Dr. Seth Smith, Dr. Brian Welch, Dr. Adam Anderson, and Dr. Victoria Morgan are also recognized for their input concerning development of the reduced-FOV techniques and the applied testing methods.

References

1. Feinberg DA, Hoenninger JC, Crooks LE, Kaufman L, Watts JC, Arakawa M. Inner volume MR imaging: technical concepts and their application. Radiology. 1985; 156:743–747. [PubMed: 4023236]
2. Le Roux P, Gilles RJ, McKinnon GC, Carlier PG. Optimized outer volume suppression for single-shot fast spin-echo cardiac imaging. J Magn Reson Imaging. 1998; 8:1022–1032. [PubMed: 9786138]
3. Luo Y, de Graaf RA, DelaBarre L, Tannus A, Garwood M. BISTRO: an outer-volume suppression method that tolerates RF field inhomogeneity. Magn Reson Med. 2001; 45:1095–1102. [PubMed: 11378888]
4. von Morze C, Kelley DA, Shepherd TM, Banerjee S, Xu D, Hess CP. Reduced field-of-view diffusion-weighted imaging of the brain at 7 T. Magnetic resonance imaging. 2010; 28:1541–1545. [PubMed: 20850242]
5. Jeong EK, Kim SE, Guo J, Kholmovski EG, Parker DL. High-resolution DTI with 2D interleaved multislice reduced FOV single-shot diffusion-weighted EPI (2D ss-rFOV-DWEPI). Magn Reson Med. 2005; 54:1575–1579. [PubMed: 16254946]
6. Finsterbusch J. Fast-spin-echo imaging of inner fields-of-view with 2D-selective RF excitations. J Magn Reson Imaging. 31:1530–1537. [PubMed: 20512911]
7. Dowell NG, Jenkins TM, Ciccarelli O, Miller DH, Wheeler-Kingshott CA. Contiguous-slice zonally oblique multislice (CO-ZOOM) diffusion tensor imaging: examples of in vivo spinal cord and optic nerve applications. J Magn Reson Imaging. 2009; 29:454–460. [PubMed: 19161202]
8. Mitsouras D, Mulkern RV, Rybicki FJ. Strategies for inner volume 3D fast spin echo magnetic resonance imaging using nonselective refocusing radio frequency pulses. Med Phys. 2006; 33:173–186. [PubMed: 16485424]
9. Wheeler-Kingshott CA, Parker GJ, Symms MR, Hickman SJ, Tofts PS, Miller DH, Barker GJ. ADC mapping of the human optic nerve: increased resolution, coverage, and reliability with CSF-suppressed ZOOM-EPI. Magnetic resonance in medicine: official journal of the Society of Magnetic Resonance in Medicine / Society of Magnetic Resonance in Medicine. 2002; 47:24–31. [PubMed: 11754439]
10. Finsterbusch J. High-resolution diffusion tensor imaging with inner field-of-view EPI. J Magn Reson Imaging. 2009; 29:987–993. [PubMed: 19306448]
11. Saritas EU, Cunningham CH, Lee JH, Han ET, Nishimura DG. DWI of the spinal cord with reduced FOV single-shot EPI. Magn Reson Med. 2008; 60:468–473. [PubMed: 18666126]
12. Wilm BJ, Svensson J, Henning A, Pruessmann KP, Boesiger P, Kollias SS. Reduced field-of-view MRI using outer volume suppression for spinal cord diffusion imaging. Magn Reson Med. 2007; 57:625–630. [PubMed: 17326167]
13. Pfeuffer J, van de Moortele PF, Yacoub E, Shmuel A, Adriany G, Andersen P, Merkle H, Garwood M, Ugurbil K, Hu X. Zoomed functional imaging in the human brain at 7 Tesla with simultaneous high spatial and high temporal resolution. Neuroimage. 2002; 17:272–286. [PubMed: 12482083]
14. Zelinski AC, Angelone LM, Goyal VK, Bonmassar G, Adalsteinsson E, Wald LL. Specific absorption rate studies of the parallel transmission of inner-volume excitations at 7T. Journal of magnetic resonance imaging: JMRI. 2008; 28:1005–1018. [PubMed: 18821601]
15. Heidemann RM, Ivanov D, Trampel R, Fasano F, Meyer H, Pfeuffer J, Turner R. Isotropic submillimeter fMRI in the human brain at 7 T: Combining reduced field-of-view imaging and partially parallel acquisitions. Magn Reson Med. 2012

16. Heidemann RM, Anwander A, Feiweier T, Knosche TR, Turner R. k-space and q-space: combining ultra-high spatial and angular resolution in diffusion imaging using ZOOPPA at 7 T. Neuroimage. 2012; 60:967–978. [PubMed: 22245337]
17. Wargo CJ, Gore JC. Localized high-resolution DTI of the human midbrain using single-shot EPI, parallel imaging, and outer-volume suppression at 7T. Magnetic resonance imaging. 2013
18. Pruessmann KP, Weiger M, Scheidegger MB, Boesiger P. SENSE: sensitivity encoding for fast MRI. Magn Reson Med. 1999; 42:952–962. [PubMed: 10542355]
19. Lustig M, Donoho D, Pauly JM. Sparse MRI: The application of compressed sensing for rapid MR imaging. Magn Reson Med. 2007; 58:1182–1195. [PubMed: 17969013]
20. Finsterbusch J, Frahm J. Half-Fourier single-shot STEAM MRI. Magn Reson Med. 2002; 47:611–615. [PubMed: 11870850]
21. Xu Y, Haacke EM. Partial Fourier imaging in multi-dimensions: a means to save a full factor of two in time. Journal of magnetic resonance imaging: JMRI. 2001; 14:628–635. [PubMed: 11747016]
22. Balchandani P, Khalighi MM, Glover G, Pauly J, Spielman D. Self-refocused adiabatic pulse for spin echo imaging at 7 T. Magn Reson Med. 2012; 67:1077–1085. [PubMed: 21954048]
23. Moore J, Jankiewicz M, Anderson AW, Gore JC. Slice-selective excitation with B(1)(+)-insensitive composite pulses. Journal of Magnetic Resonance. 2012; 214:200–211. [PubMed: 22177383]
24. Moore J, Jankiewicz M, Zeng H, Anderson AW, Gore JC. Composite RF pulses for B1+-insensitive volume excitation at 7 Tesla. J Magn Reson. 205:50–62. [PubMed: 20451430]
25. Katscher U, Bornert P. Parallel RF transmission in MRI. NMR Biomed. 2006; 19:393–400. [PubMed: 16705630]
26. Katscher U, Bornert P, Leussler C, van den Brink JS. Transmit SENSE. Magn Reson Med. 2003; 49:144–150. [PubMed: 12509830]
27. Sersa II, Macura S. Excitation of Arbitrary Shapes in Nuclear Magnetic Resonance by a Random Walk in Discrete k Space. J Magn Reson B. 1996; 111:186–188. [PubMed: 8661279]
28. Moore J, Jankiewicz M, Anderson AW, Gore JC. B1+-insensitive slice-selective pulses constructed from optimized non-selective composite waveforms. Proc Int Soc Magn Reson Med. 2011; 19:2912.
29. Boehlen JM, Ray M, Bodenhausen G. Refocusing with Chirped Pulses for Broadband Excitation without Phase Dispersion. Journal of Magnetic Resonance. 1989; 84:191–197.
30. Schulte RF, Henning A, Tsao J, Boesiger P, Pruessmann KP. Design of broadband RF pulses with polynomial-phase response. Journal of Magnetic Resonance. 2007; 186:167–175. [PubMed: 17331765]
31. Schulte RF, Tsao J, Boesiger P, Pruessmann KP. Equi-ripple design of quadratic-phase RF pulses. Journal of Magnetic Resonance. 2004; 166:111–122. [PubMed: 14675826]
32. Symms, MR.; Wheeler-Kingshott, CA.; Parker, GJM.; Barker, GJ. Z Onally-magnified Oblique Multislice (ZOOM) EPI; Proc Int Soc Magn Reson Med; Denver, United States. 2000;
33. Kim SE, Jeong EK, Shi XF, Morrell G, Treiman GS, Parker DL. Diffusion-weighted imaging of human carotid artery using 2D single-shot interleaved multislice inner volume diffusion-weighted echo planar imaging (2D ss-IMIV-DWEPI) at 3T: diffusion measurement in atherosclerotic plaque. Journal of magnetic resonance imaging: JMRI. 2009; 30:1068–1077. [PubMed: 19856440]
34. Bottomley, PA. Selective Volume Method for Performing Localized NMR Spectroscopy. General Electric Company; United States: 1984.
35. Reese TG, Heid O, Weisskoff RM, Wedeen VJ. Reduction of eddy-current-induced distortion in diffusion MRI using a twice-refocused spin echo. Magn Reson Med. 2003; 49:177–182. [PubMed: 12509835]
36. Pisani L, Bammer R, Glover G. Restricted field of view magnetic resonance imaging of a dynamic time series. Magn Reson Med. 2007; 57:297–307. [PubMed: 17260360]
37. Hardy CJ, et al. Spatial Localization in Two Dimensions Using NMR Designer Pulses. Journal of Magnetic Resonance. 1989; 82:647–654.

38. Pauly J, et al. A k-space Analysis of Small-Tip-Angle Excitation. Journal of Magnetic Resonance. 1989; 81:43–56.

39. Hardy CJ, Bottomley PA, Roemer PB. Off-axis spatial localization with frequency modulated nuclear magnetic resonance rotating (ρ) pulses. J Appl Phys. 1988; 63:4741–4743.

40. Friedman L, Glover GH. Report on a multicenter fMRI quality assurance protocol, Journal of magnetic resonance imaging. JMRI. 2006; 23:827–839. [PubMed: 16649196]

41. Scheenen TW, Heerschap A, Klomp DW. Towards 1H-MRSI of the human brain at 7T with slice-selective adiabatic refocusing pulses. Magma. 2008; 21:95–101. [PubMed: 18210177]

42. Adriany G, Van de Moortele PF, Wiesinger F, Moeller S, Strupp JP, Andersen P, Snyder C, Zhang X, Chen W, Pruessmann KP, Boesiger P, Vaughan T, Ugurbil K. Transmit and receive transmission line arrays for 7 Tesla parallel imaging. Magn Reson Med. 2005; 53:434–445. [PubMed: 15678527]

43. Valette J, Park JY, Grohn O, Ugurbil K, Garwood M, Henry PG. Spectroscopic imaging with volume selection by unpaired adiabatic pi pulses: theory and application. Journal of Magnetic Resonance. 2007; 189:1–12. [PubMed: 17851103]

44. Conolly S, Glover G, Nishimura D, Macovski A. A reduced power selective adiabatic spin-echo pulse sequence. Magn Reson Med. 1991; 18:28–38. [PubMed: 2062239]

45. Wheeler-Kingshott CA, Trip SA, Symms MR, Parker GJ, Barker GJ, Miller DH. In vivo diffusion tensor imaging of the human optic nerve: pilot study in normal controls. Magn Reson Med. 2006; 56:446–451. [PubMed: 16791864]

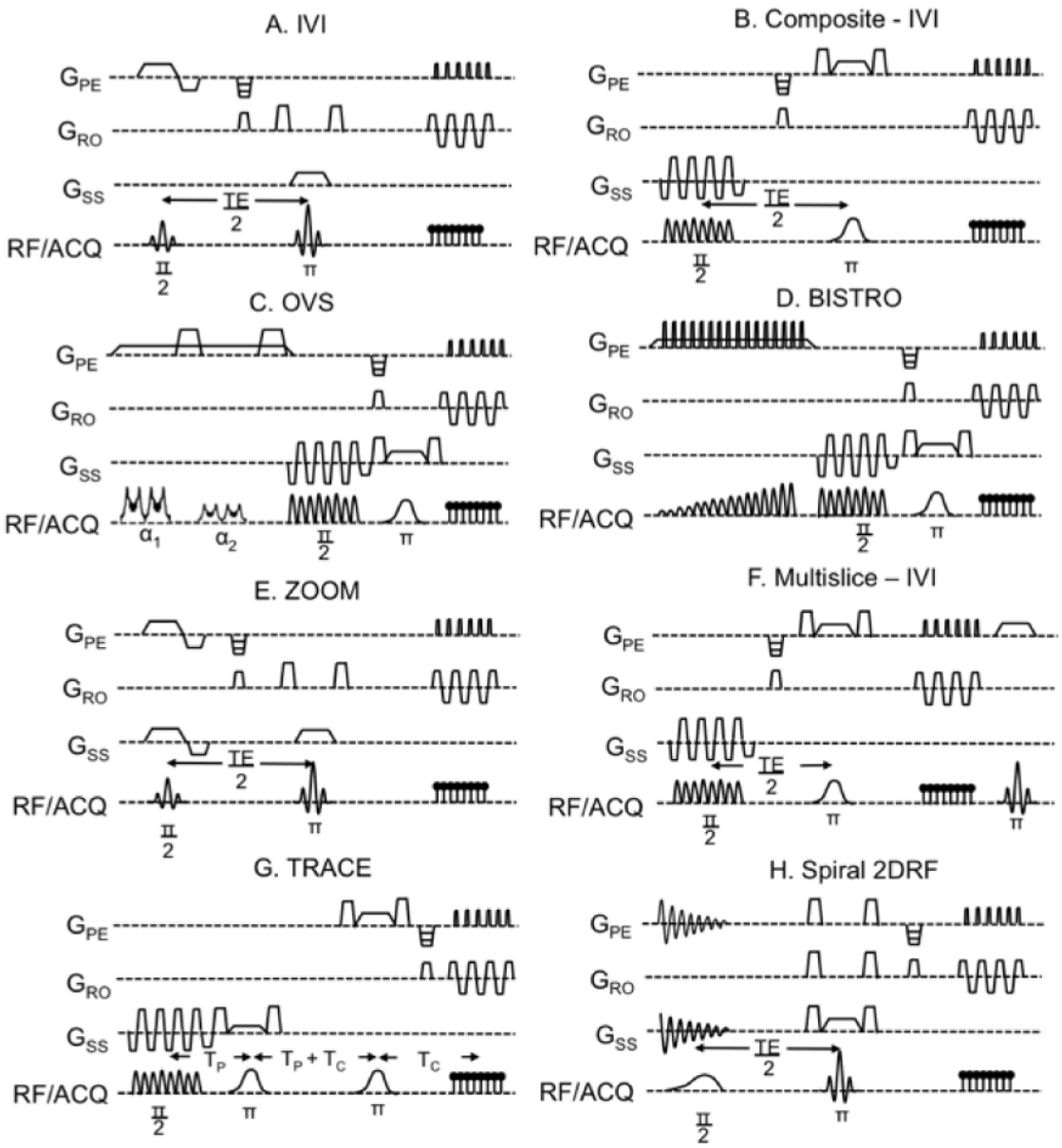

Figure 1.

Pulse sequences for each reduced-FOV methods tested: A.) IVI, B.) CE-IVI, C.) OVS, D.) BISTRO, E.) ZOOM, F.) MS-IVI, G.) TRACE, and H.) Spiral 2DRF-IVI.

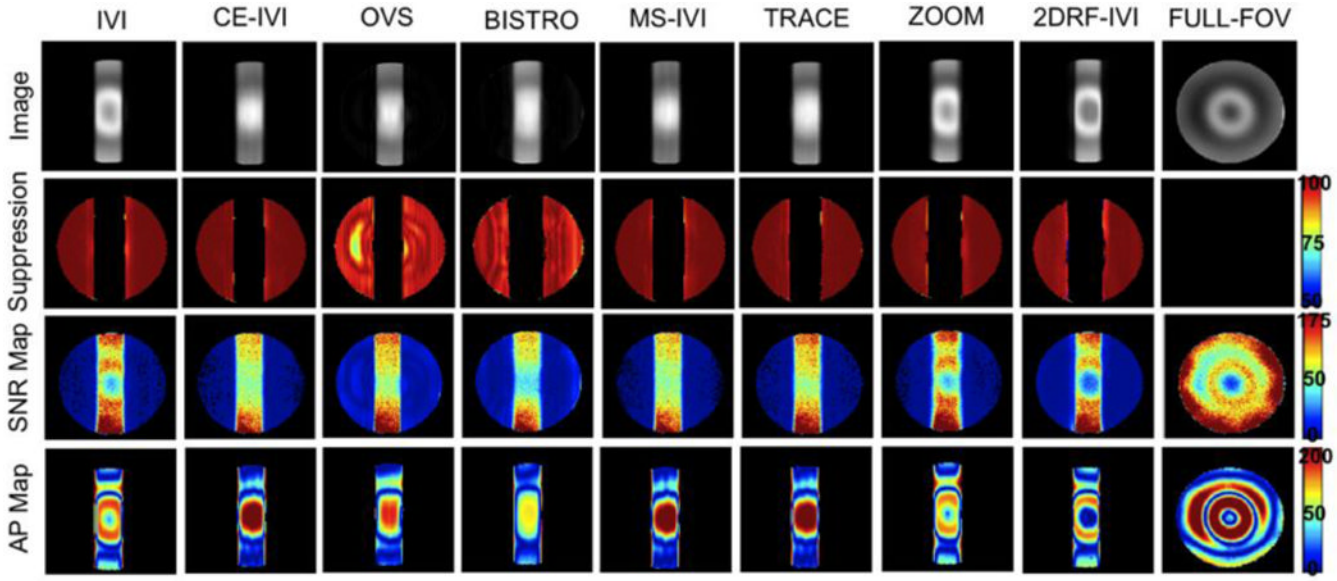

Figure 2.
Images of a slab excitation in a FBIRN phantom for all eight reduced-FOV methods and a full-FOV scan and maps of percent suppression, SNR, and artifact power.

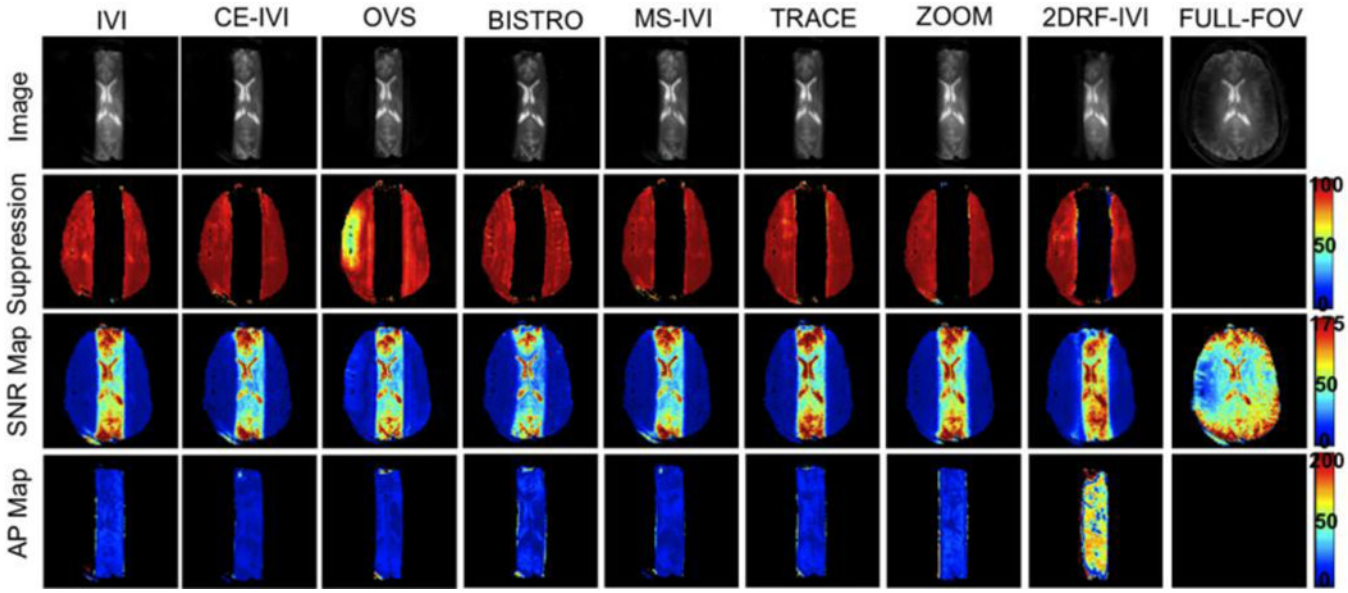

Figure 3.
Images of a slab excitation in a human subject for all eight reduced-FOV methods and a full-FOV scan and maps of percent suppression, SNR, and artifact power.

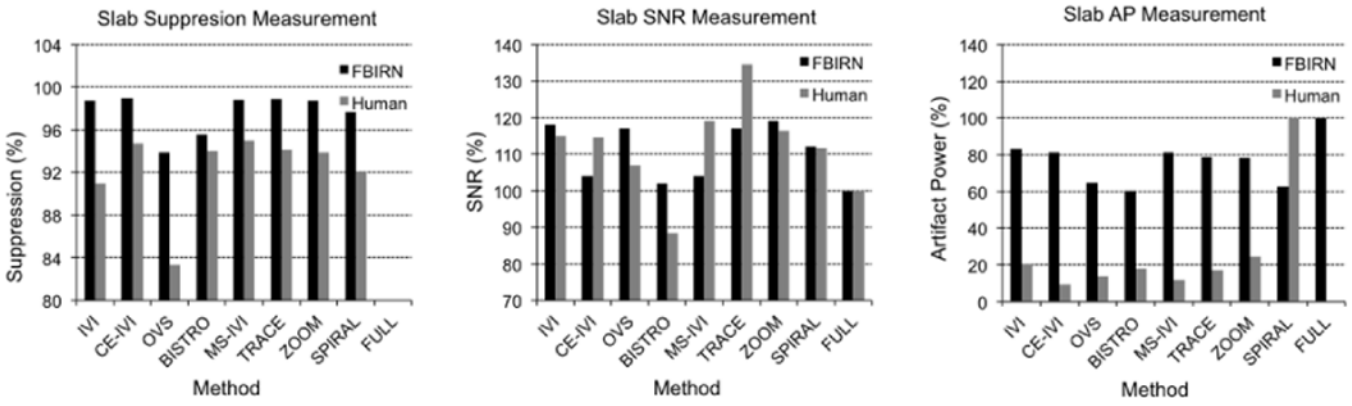

Figure 4.

Measured mean SNR, artifact power, and percent suppression statistics for slab excitations in FBIRN and human for reduced-FOV methods relative to full-FOV.

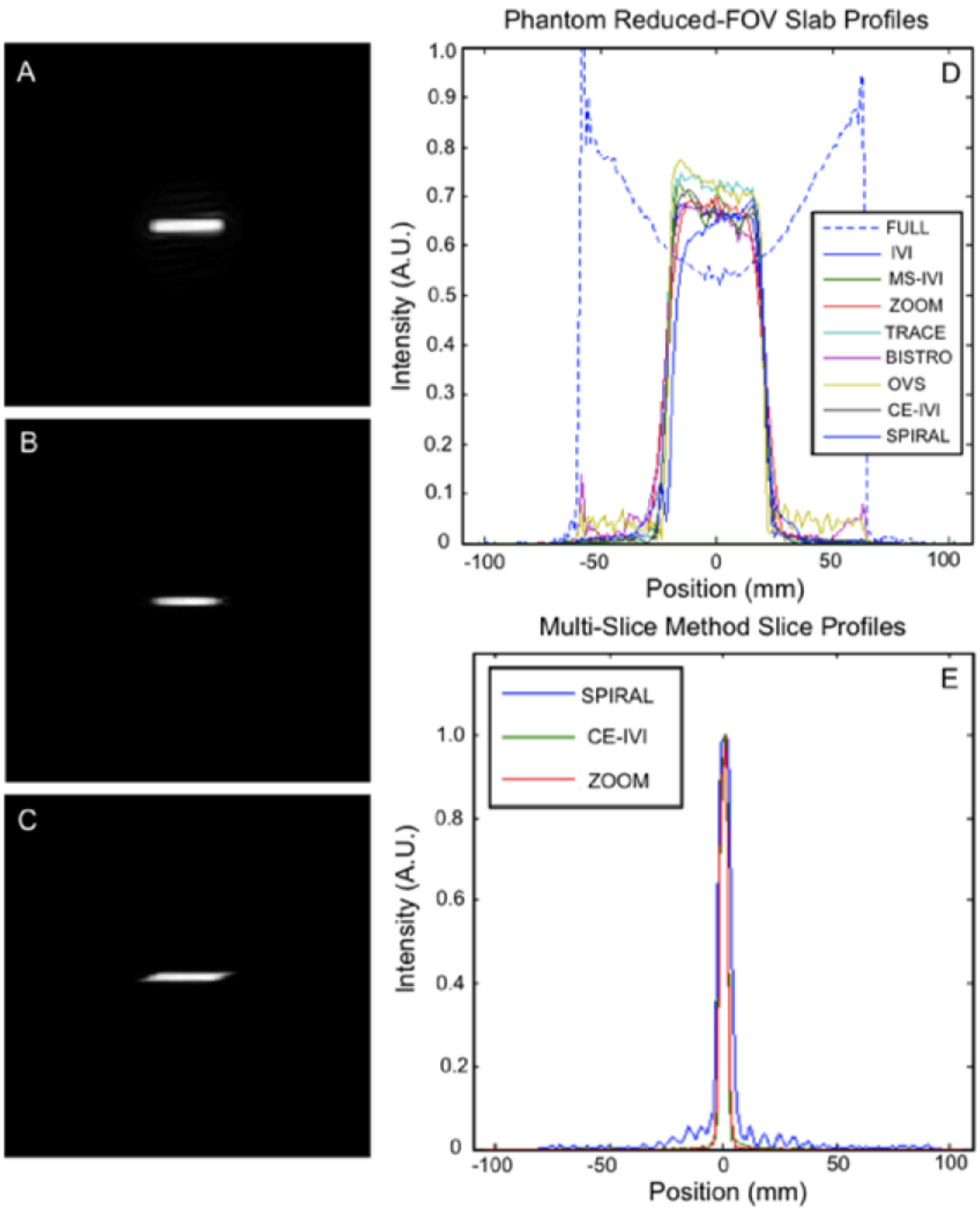

Figure 5.
In plane slice profiles for A.) rectangular spiral 2DRF pulse, B.) composite excitation, and C.) ZOOM rotated excitation pulse. E.) Cross-sectional profile for the slab excited by each reduced-FOV method. F.) Profile across pulses A through B.

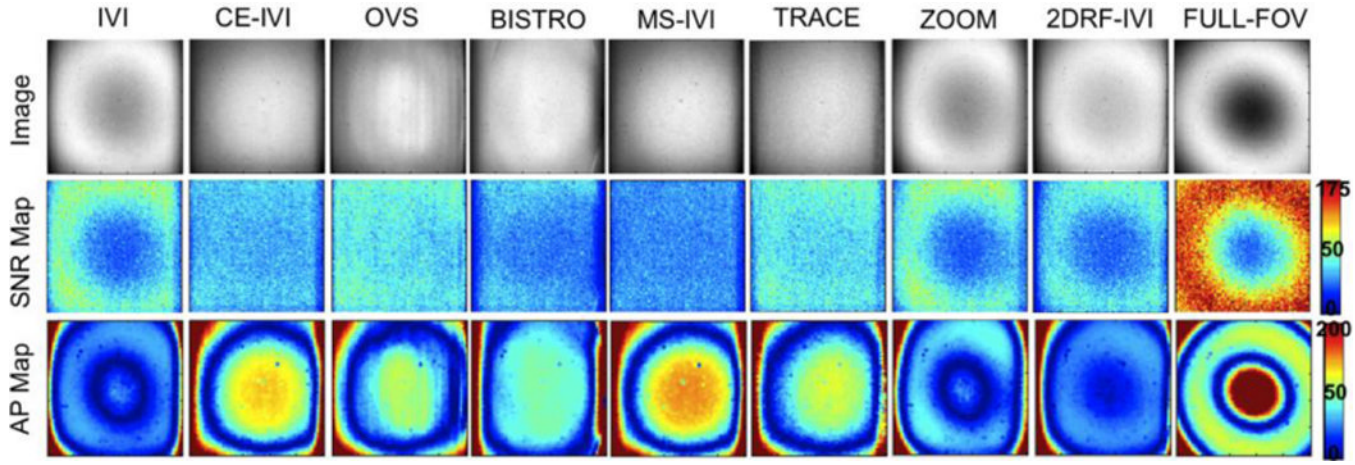

Figure 6.
Images of a small FOV excitation in an FBIRN phantom using each reduced-FOV method and a full-FOV scan, measured SAR, and maps of SNR and artifact power.

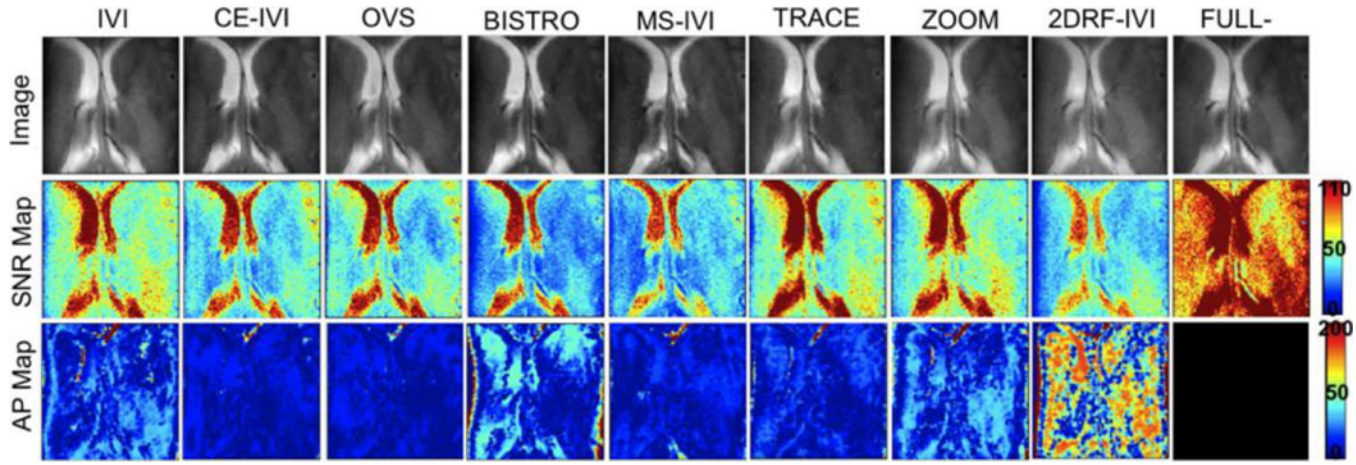

Figure 7.
Images of a small FOV excitation in a human subject using each reduced-FOV method and a full-FOV scan and corresponding maps of SNR and artifact power.

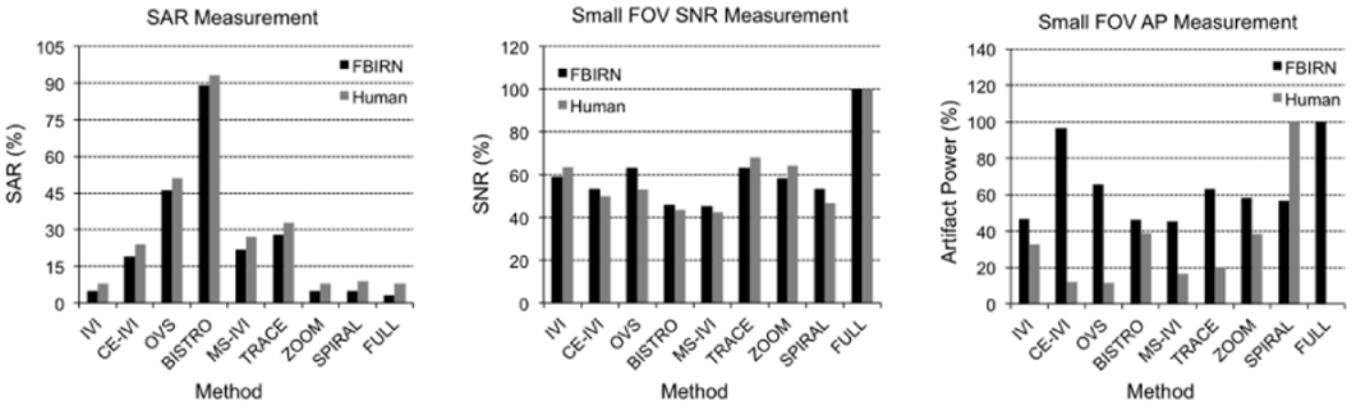

Figure 8.

Measured SAR, mean SNR, and artifact power for each reduced-FOV method and a full scan in small FOV FBIRN phantom and human subject scans.

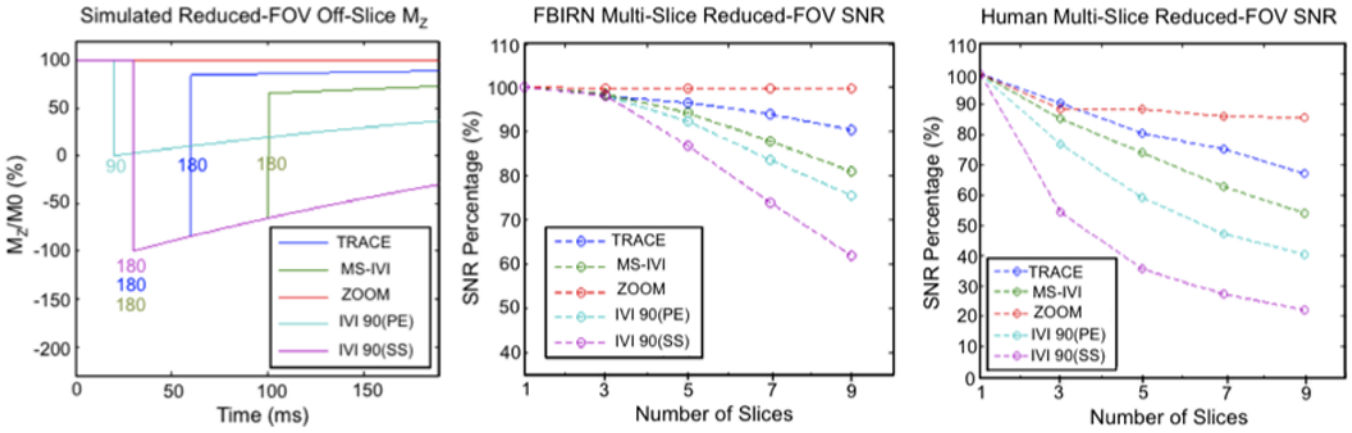

Figure 9.

Simulated off-slice magnetization using ZOOM, MS-IVI, TRACE, IVI-90(PE), and IVI-90(SS) with a multi-slice scan. Timing and angle of pulses acting on the off-slice are shown, where SS corresponds to a slice selective pulse, and PE corresponds to a phase encoding pulse. Measured loss in SNR for slice numbers ranging from 1 to 9 in an FBIRN phantom and human subject, normalized to percentage of 1 slice SNR.

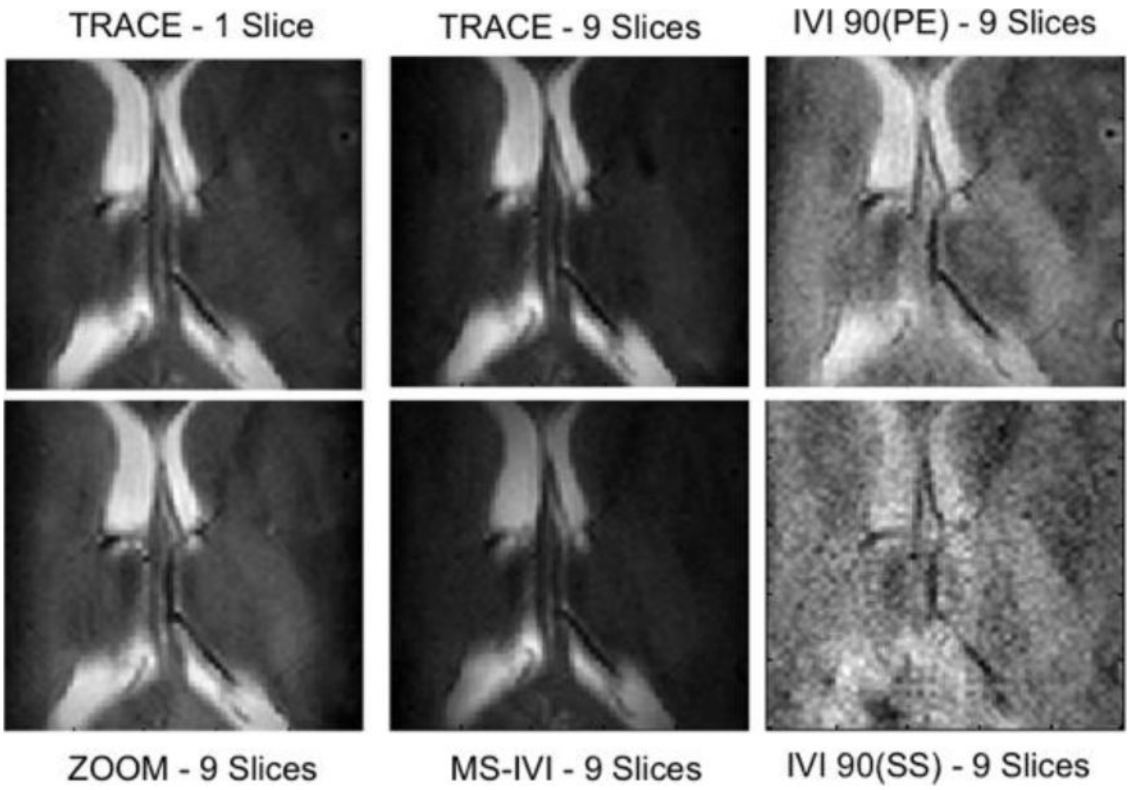

Figure 10.
Multi-slice images in a human subject using reduced-FOV methods for TRACE (1 and 9 slices), MS-IVI, IVI-90(SS), and IVI-90(PE).

Table 1

Scan parameters used to test the developed reduced-FOV methods. A.) Excitation of a slab, B.) reduction to a small FOV, and C.) reduced-FOV multi-slice.

Tesf Method		*Scan*	*EPI Factor*	*FOV (mm^2)*	*TR (ms)*	*TE (ms)*	*NSA*	**Resolution** *(mm^3)*	*WFS (pixels)*	*Slices*
A	Slab Data	SE-EPI	27	210 × 210	3000	32	1	1.0 × 1.0 × 3	12	1
B	Small FOV	SE-EPI	11	60 × 60	3000	45	2	0.6 × 0.6 × 3	12	1
C	Multi-Slice	SE-EPI	15	60 × 60	4200	45	2	0.3 × 0.8 × 4	12	1,3,5,7,9